Immunity, Vol. 11, 45–56, July, 1999, Copyright ©1999 by Cell Press

Four A6-TCR/Peptide/HLA-A2 Structures that Generate Very Different T Cell Signals Are Nearly Identical

Yuan-Hua Ding*, Brian M. Baker*, David N. Garboczi‡, William E. Biddison,§ and Don C. Wiley*†‖
*Department of Molecular and Cellular Biology
Harvard University
†Howard Hughes Medical Institute
Cambridge, Massachusetts 02138
‡Structural Biology Section
National Institute of Allergy and Infectious Diseases
National Institutes of Health
Rockville, Maryland 20852
§Molecular Immunology Section
Neuroimmunology Branch
National Institute of Neurological Disorders and Stroke
National Institutes of Health
Bethesda, Maryland 20892

Summary

The interactions of three singly substituted peptide variants of the HTLV-1 Tax peptide bound to HLA-A2 with the A6 T cell receptor have been studied using T cell assays, kinetic and thermodynamic measurements, and X-ray crystallography. The three peptide/MHC ligands include weak agonists and antagonists with different affinities for TCR. The three-dimensional structures of the three A6-TCR/peptide/HLA-A2 complexes are remarkably similar to each other and to the wild-type agonist complex, with minor adjustments at the interface to accommodate the peptide substitutions (P6A, V7R, and Y8A). The lack of correlation between structural changes and the type of T cell signals induced provides direct evidence that different signals are not generated by different ligand-induced conformational changes in the αβTCR.

Introduction

Peptides with single amino acid substitutions (altered peptide ligands [APL]) presented by the same MHC molecule can induce quantitatively and qualitatively different signals when recognized by the same T cell receptor (reviewed in Sloan-Lancaster and Allen, 1996). A strong agonist ligand provided at very low concentrations induces T cell cytotoxicity, TCR downregulation, the production of cytokines, and hyperphosphorylation of the TCR related ζ chain and the tyrosine kinase ZAP-70. Weak agonists have the same effects but at 100- to 1000-fold higher ligand concentrations. Some APL are antagonists: they inhibit T cell responses by agonists and are characterized by specific patterns of phosphorylation of ZAP-70 and ζ chains (Ljunggren et al., 1990; Sloan-Lancaster et al., 1994; Madrenas et al., 1995; Sloan-Lancaster and Allen, 1996).

The molecular mechanism for how TCR binding to different APL generates different responses is unclear. Models include the induction of different TCR conformations or differences in the rates of formation, disassembly, or stability of TCR oligomers (reviewed in Sloan-Lancaster and Allen, 1996; Davis et al., 1998). Studies from a number of laboratories suggest that the half-life of a TCR/peptide/MHC complex correlates with the type of signal generated: the longest half-lives generate agonist signals (reviewed in Davis et al., 1998).

X-ray crystallographic structure determinations of TCR and TCR/peptide/MHC class I complexes have demonstrated that TCRs undergo induced fitting to optimize contacts to ligand and supported certain concepts for signaling (Garboczi et al., 1996a; Garcia et al., 1996, 1998; Ding et al., 1998). The comparison of the structures of two different human TCR bound to the same peptide/MHC ligand has shown how very different TCR sequences can recognize the same antigen, using slightly different diagonal binding modes, and both produce full T cell activation (Ding et al., 1998).

The A6 TCR studied here was expressed by a cytolytic $CD8^+$ T cell clone derived from an HTLV-1-infected patient with the neural degenerative disorder HAM/TSP (Roman and Osame, 1988; Utz et al., 1996). The TCR is specific for the Tax peptide (LLFGYPVYV) of HTLV-1 presented by HLA-A2. We have assayed a number of T cell functions of the Tax peptide and many single amino acid variants of Tax (Garboczi et al., 1996a; Ding et al., 1998; Hausmann et al., 1999).

Here, we present data for three peptides, P6A, V7R, and Y8A, which include one weak agonist and two weak antagonists. The weak antagonists inhibit T cell function when present at 1000-fold molar excess over the Tax peptide. Despite the different T cell signals that these APL peptides induce, we could crystallize and determine the structures of all of them complexed with the A6-TCR and HLA-A2. We compare the structures of these three complexes with the agonist complex, A6-TCR/Tax/HLA-A2, whose structure was reported earlier (Garboczi et al., 1996a). The structures provide a direct visualization of cross-reactivity that generates different intracellular signals. Cross-reactivity is achieved by small structural adjustments: induced fits, where TCR, peptide, and MHC residues rearrange to better accommodate the altered peptide. There is, however, no correlation between the types of minor structural adjustments at the interface and beyond the interface with the type of signal generated inside the cell.

Results and Discussion

Three Singly Modified Tax Peptides Generate Different T Cell Responses

The capacity of variant Tax peptides V7R, P6A, and Y8A, which contained single substitutions, to produce different biological effects upon interaction with the

‖To whom correspondence should be addressed (e-mail: dcwadmin@crystal.harvard.edu).

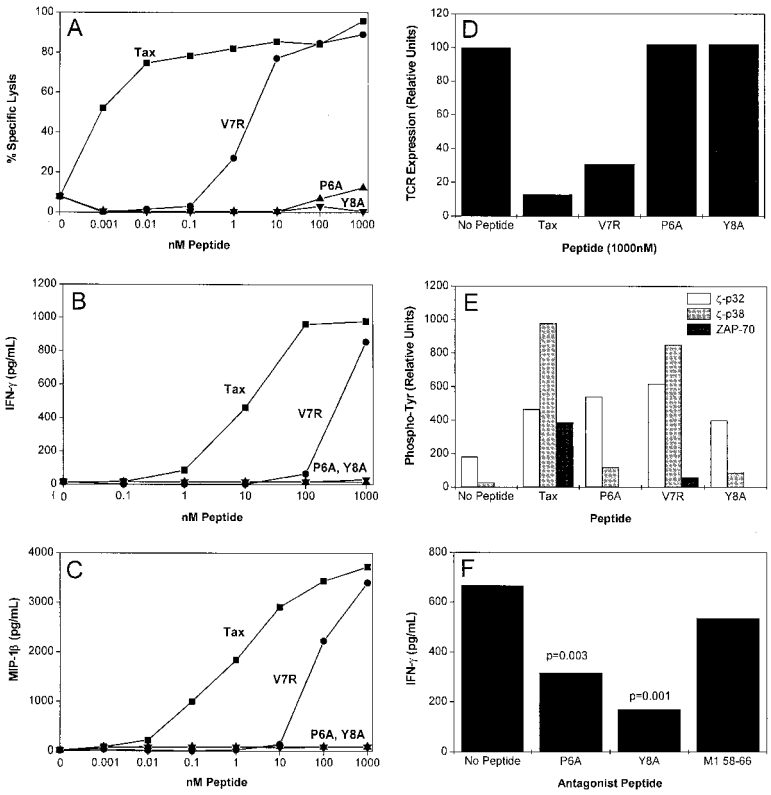

G

	Cytotoxicity	IFN-γ	MIP-1β	TCR Downreg.	p32-ζ-P	p38-ζ-P	ZAP-70-P
Tax	++	++	++	++	++	++	++
P6A	–	–	–	–	+	+/–	–
V7R	+/–	+/–	+	+/–	+	+	+/–
Y8A	–	–	–	–	+	+/–	–

Figure 1. T Cell Assays

(A–C) Reactivity of HTLV-1 Tax-specific clone 2G4 to altered Tax peptides. 2G4 was assayed for its capacity to lyse (A) or secrete IFNγ (B) or MIP-1β (C) when presented with APC pulsed with peptides. Tax, square; V7R, closed circle; P6A, closed triangle; Y8A, upside down closed triangle.

(D) Cell surface TCR downmodulation induced by variant Tax peptides. 2G4 T cells were exposed to APC pulsed with 1 μM of the indicated peptides for 5 hr at 37°C, washed, and cell surface TCR was quantitated by flow cytometry. Units are the percentage mean fluorescence intensity of TCR expression relative to T cells cultured with APCs pulsed with no peptide.

(E) Differential TCR signaling patterns induced by variant Tax peptides. 2G4 T cells were exposed to APC pulsed with 10 μM of peptide for 5 min at 37°C. Tyrosine phosphorylation of ζ chains and ZAP-70 was detected in the ZAP-70 immunoprecipitated complex (see the Experimental Procedures). Y-axis values are relative densitometer units for bands corresponding to p32ζ, p38ζ, and ZAP-70.

(F) P6A and Y8A antagonize secretion of IFNγ induced by Tax. Mitomycin C–treated APC were pulsed with 1000 nM of peptide for 2 hr at 37°C, washed, and incubated with 2G4 cells for 1 hr at 37°C. Tax peptide was then added at a final concentration of 1 nM and incubated for 48 hr. Supernatants were assayed for IFNγ. Quantitative differences were analyzed by the Student's t test.

(G) Summary of (A) to (F).

A6-TCR-bearing T cell clone 2G4 was assessed by cytotoxicity, cytokine and chemokine secretion, cell surface TCR downmodulation (Valitutti et al., 1995), and phosphorylation of TCR-associated signaling molecules (Sloan-Lancaster et al., 1994; Madrenas et al., 1995; Sloan-Lancaster and Allen, 1996). The variant Tax peptide V7R could induce cytotoxicity (Figure 1A) and IFNγ (Figure 1B) and MIP-1β (Figure 1C) secretion with approximately 10- to 100-fold more V7R peptide required to achieve a comparable level of effector function as that induced by the Tax peptide. In contrast, Tax peptides P6A and Y8A were unable to induce any detectable effector functions even at a concentration of 1000 nM (Figures 1A–1C). These results demonstrate that the V7R peptide is a weak agonist, whereas the P6A and Y8A peptides could be null ligands.

While the Tax peptide induced nearly complete cell surface TCR downmodulation following exposure to peptide-pulsed antigen-presenting cells (APCs) (Valitutti et al., 1995), neither P6A nor Y8A was able to induce any detectable cell surface TCR downmodulation (Figure 1D). Peptide V7R induced TCR downmodulation but to a somewhat lesser extent than the Tax peptide (Figure 1D). These results again indicate that the V7R peptide but not P6A or Y8A is able to functionally engage the A6-TCR.

To examine whether the P6A and Y8A peptides might induce an antagonist response (Sloan-Lancaster and Allen, 1996), clone 2G4 was exposed to APC pulsed with either the P6A and Y8A peptides and a negative control HLA-A2 epitope influenza M1 58-66 and then incubated with 1 nM of the Tax peptide. The effect of preexposure to candidate antagonist peptides on subsequent interaction with the Tax peptide was quantitated by IFNγ secretion. The results (Figure 1F) demonstrate that the P6A and Y8A peptides but not the M1 58-66 peptide produced a significant reduction in IFNγ secretion. Similar results were obtained when APCs were prepulsed with 1 nM Tax and then cultured with 1000 nM P6A or Y8A (data not shown). No antagonist effect was seen at 10-fold lower concentration of either P6A or Y8A (data not shown). These results indicate that the P6A and Y8A peptides are very weak antagonists (only effective when at 1000-fold higher concentration than the agonist).

To confirm the classification of V7R as a weak agonist and P6A and Y8A as antagonist peptides for the A6 TCR, we examined the ζ chain and ZAP-70 phosphorylation patterns induced in 2G4 T cells by these peptides (Sloan-Lancaster et al., 1994; Madrenas et al., 1995; Sloan-Lancaster and Allen, 1996) (Figure 1E). The Tax peptide induced the characteristic agonist signaling pattern (Sloan-Lancaster et al., 1994; Madrenas et al., 1995; Sloan-Lancaster and Allen, 1996): phosphorylation of

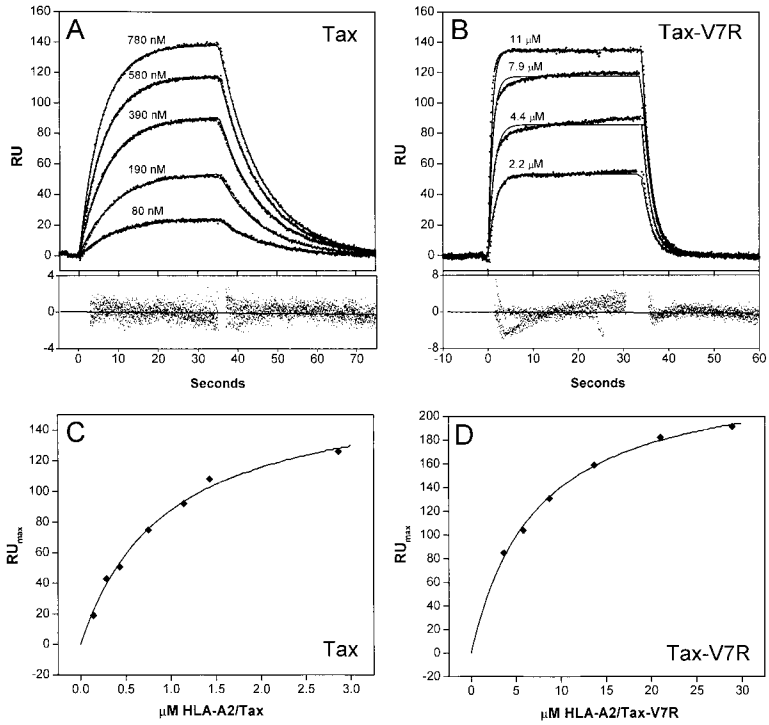

Figure 2. Biacore Data

(A and B) Kinetic binding experiments for HLA-A2 with wild-type Tax (A) and Tax-V7R (B). Solid lines are a fit to a 1:1 binding model. Concentrations of injected protein are indicated. Residuals are below plots.

(C and D) Equilibrium binding experiments (on separate surfaces from [A] and [B]) for HLA-A2 with wild-type Tax (C) and Tax-V7R (D). Solid lines are a fit to a 1:1 binding model.

(E) Fitted parameters from (A)–(D). Errors in kinetic terms are standard deviations from multiple experiments; errors in $t_{1/2}$ and k_{off}/k_{on} are propagated from these values. Errors in $K_{D,eq}$ are standard deviations from the nonlinear fits. No binding was seen for HLA-A2 with Tax-P6A or Tax-Y8A.

E

	k_{on} (M^{-1} s^{-1})	k_{off} (s^{-1})	$t_{1/2}$ (s)	k_{off}/k_{on} (μM)	$K_{D,eq}$ (μM)
Tax	$1.1 \pm 0.1 \times 10^5$	0.093 ± 0.002	7.5 ± 0.2	0.82 ± 0.08	0.91 ± 0.09
V7R	$5.8 \pm 0.9 \times 10^4$	0.47 ± 0.03	1.5 ± 0.1	8.1 ± 1.4	7.2 ± 0.5
P6A	n.d.	n.d.	–	–	n.d.
Y8A	n.d.	n.d.	–	–	n.d.

TCR-associated ζ chain producing more of the hyperphosphorylated p38ζ than the hypophosphorylated p32ζ, and phosphorylation of ZAP-70. The V7R peptide induced the weak agonist pattern of TCR signaling (Sloan-Lancaster et al., 1994; Madrenas et al., 1995; Sloan-Lancaster and Allen, 1996): increased p32ζ relative to p38ζ and almost undetectable levels of ZAP-70 phosphorylation. Both P6A and Y8A showed a characteristic antagonist pattern: p32ζ phosphorylation but almost no detectable p38ζ and no detectable ZAP-70 phosphorylation.

The Three Singly Modified Tax Peptides Have Different Kinetic and Thermodynamic Effects In Vitro

Biacore has been used extensively to characterize TCR-MHC interactions, providing interaction affinities and often kinetic rate constants (e.g., Davis et al., 1998). Representative kinetic and equilibrium data for A6-TCR binding to HLA-A2 complexed with wild-type Tax and Tax-V7R peptides are shown in Figure 2. For the kinetic experiments, the data were fit to a 1:1 binding model over the entire injection period (Figures 1A and 1B; but see the Experimental Procedures). Good agreement is observed between the affinities determined kinetically (the ratio of k_{off} to k_{on}) and those determined by equilibrium measurements (Figures 1C and 1D). Figure 1E summarizes the data. The A6-TCR binds HLA-A2/wild-type Tax with a K_D of approximately 0.9 μM. This is composed of an on-rate of 1×10^5 $M^{-1}s^{-1}$ and an off-rate of 0.09 s^{-1}, or a half-life of approximately 8 sec. The V7R interaction is almost an order of magnitude weaker, with a K_D of approximately 8 μM, reflecting an on-rate of 6×10^4 $M^{-1}s^{-1}$ and an off-rate of 0.5 s^{-1}, or a half-life of 1.5 sec.

For the interaction involving P6A and Y8A, no binding was detectable in either kinetic or equilibrium mode. However, equilibrium analytical ultracentrifugation studies of the P6A indicate an affinity of approximately 100 μM, approximately 100-fold weaker than Tax (B. M. B. and D. C. W., unpublished data).

Altogether, the binding results are consistent with the T cell assays, with the most potent TCR ligand (HLA-A2/wild-type Tax) having the strongest affinity and the longest half-life, followed by the weakly activating V7R ligand with a weaker affinity and shorter half-life, and, finally, by the P6A and Y8A ligands, which bind very weakly. These effects are not likely to result from alterations in the affinity of the peptides for the MHC, as Val-7 and Tyr-8 make little contact with the MHC in the free HLA-A2/Tax structure (Madden et al., 1993), and Tax-P6A/HLA-A2 is a strong agonist ligand for the TCR clone B7 (Hausmann et al., 1999).

Three-Dimensional Structure Determinations of Three TCR/Tax-APL/MHC Complexes

TCR/peptide/MHC complexes were produced by expressing the ectodomain of each subunit, α and β of

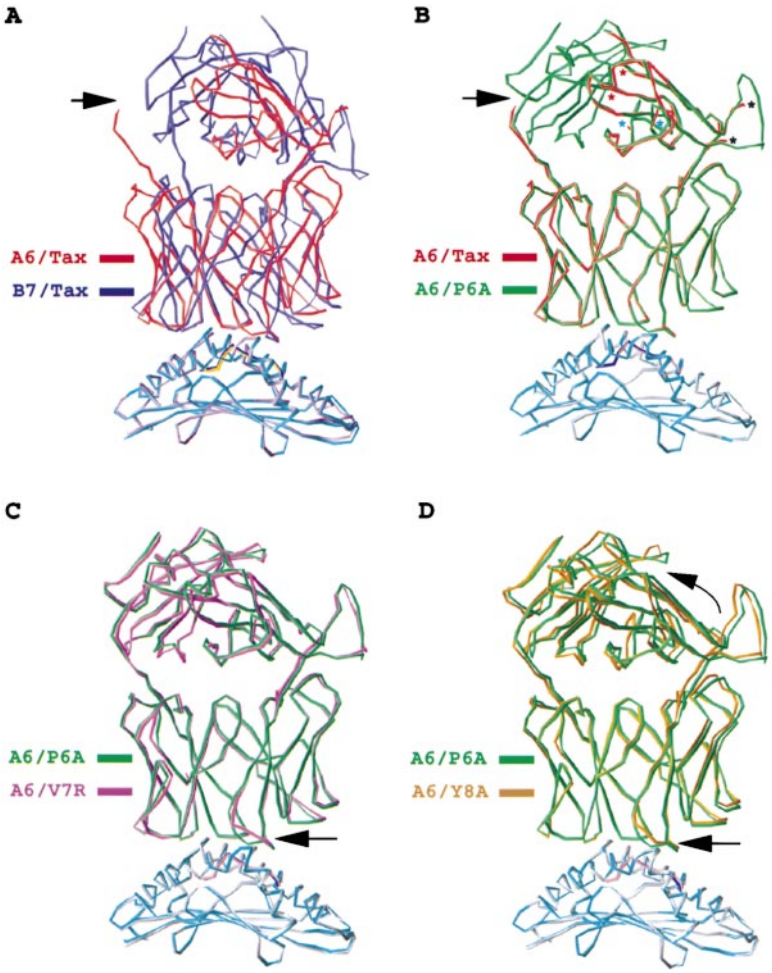

Figure 3. Comparison of TCR/Tax/HLA-A2 and TCR/Tax-APL/HLA-A2 Complexes with the α1 and β2 Domains Superimposed

(A) Two different TCRs, A6 (red) and B7 (blue). An arrow shows the location of the Cα domain that was missing in the A6-TCR/Tax/HLA-A2 structure. The pronounced difference in the A6 and B7 TCR complexes, both strong agonists, has been described (Ding et al., 1998). HLA-A2 (light blue and purple) and the bound peptide (black and yellow) are shown; the α3 domain and β2M were omitted for clarity.

(B) A6-TCR/P6A/HLA-A2 (green) and A6-TCR/Tax/HLA-A2 complex (orange). Asterisks show the locations of the three loops in the Cβ domain (right) that were disordered in the A6-TCR/Tax/HLA-A2 structure but visible in the P6A complex.

(C) A6-TCR/V7R/HLA-A2 (magenta) and A6-TCR/P6A/HLA-A2 complex (green). Arrow marks the structural difference in the CDR3 loop of the Vβ domain.

(D) A6-TCR/Y8A/HLA-A2 (orange) and A6-TCR/P6A/HLA-A2 complex (green). Straight arrow marks the structural difference in the CDR3 loop of the Vβ domain. Curved arrow indicates the sense of the small (1.8 Å) twist of the β chain. This figure was generated with RIBBONS (Carson, 1991).

the A6-TCR and heavy chain and β2m of HLA-A2, separately in bacteria. Each subunit was purified as inclusion bodies, and the TCR and MHC/peptide were folded in vitro and purified before being combined to form TCR/peptide/MHC complexes as described previously (Garboczi et al., 1992, 1996b).

The three crystal structures, P6A, V7R, and Y8A, were determined by molecular replacement and refined to 2.8 Å resolution (see the Experimental Procedures).

TCR/Tax-APL/MHC Complexes that Signal Differently Have Very Similar Structures

When the HLA-A2 α1α2 domains are superimposed, the A6-TCR molecules of all three Tax-APL complexes superimpose very closely (Figure 3). The similarity in structure is greatest in the P6A complex where, when the α1α2 domains are superimposed on the A6/Tax/HLA-A2 complex (root mean square deviation [rmsd] = 0.2 Å; for 180 Cα atoms), the TCRs are positioned almost identically (rmsd = 0.6 Å; for 320 Cα atoms) (Figure 3B). Yet, the Tax peptide causes the TCR to generate a strong agonist signal and the P6A peptide is a weak antagonist.

Both the V7R and Y8A complexes, the former a weak agonist and the latter a weak antagonist, have a similar structural difference at the CDR3 loop of the Vβ domain (Figures 3C and 3D, arrows) when compared to either of the nearly identical Tax or P6A complexes. (The figures compare the V7R [Figure 3C, magenta] and Y8A complexes [Figure 3D, orange] to the P6A complex [green], because the P6A complex is a more complete model than Tax.) In the V7R complex, the six CDR3β residues Leu-98 to Gly-101, encoded by the D region, and the N additions Arg-102 and Pro-103, are rearranged to accommodate the large V7R arginine side chain (Figure 3C, arrow). While the Cα position of Leu-98 differs by only 0.8 Å, Gly-100, Gly-101, and Arg-102 at the apex of the CDR3β loop differ substantially more; for example, Gly-101 has moved outwardly in the interface by 4.4 Å. A similar structural difference is found in the Y8A complex (Figure 3D, lower arrow), where Leu-98 also differs by 0.8 Å and the glycines at 100 and 101 have moved and may be partially disordered judging by the weak electron density at their positions. The structural differences in the V7R complex are restricted to the interface between the TCR and peptide/MHC, but in the Y8A complex the β subunit of the TCR is tilted slightly upward (~1.8 Å measured at the top of Cβ; Figure 3D, upper arrow).

There is apparently no correlation between the overall shape of the complex or the rearrangements at the interface and the type of signal generated by the TCR.

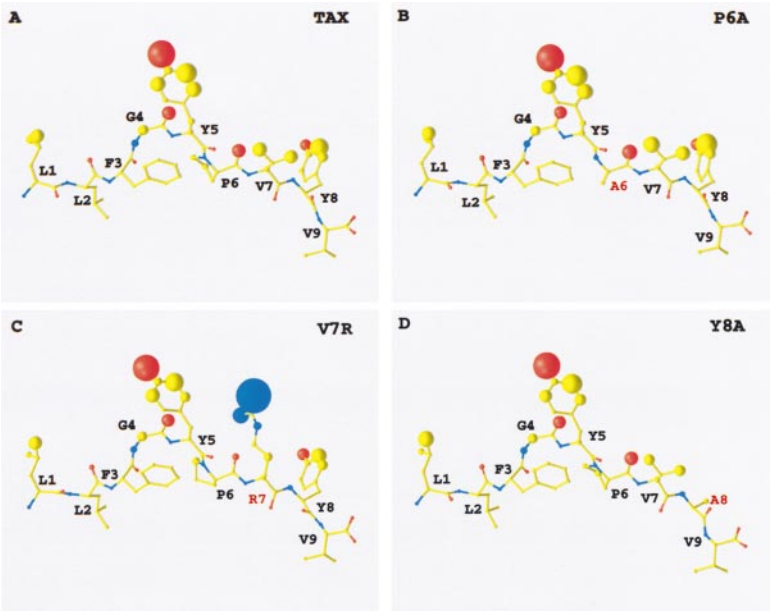

Figure 4. Surface Areas of Peptide Atoms Buried by the A6-TCR in the TCR/Peptide/MHC Interface

(A) The structure of the Tax peptide (LLFGYPVYV) in the A6-TCR/Tax/HLA-A2 complex. The radius of the large spherical atoms is shown proportional to the solvent-accessible surface of the MHC bound peptide that is buried by the TCR. Carbons are yellow, oxygens red, and nitrogens blue. Buried solvent-accessible surface area summary: total, 2073 Å^2; MHC + peptide, 1031 Å^2; TCR, 1042 Å^2; peptide alone, 336 Å^2. Areas calculated with a 1.4 Å radius probe using the program ACCESS (Scott Presnell, ZymoGenetics). Peptide represents only the peptide surface buried by the TCR.

(B) The structure of the P6A peptide represented as in (A). Summary: total, 2046 Å^2; MHC + peptide, 1024 Å^2; TCR, 1022 Å^2; peptide alone, 336 Å^2.

(C) The structure of the V7R peptide represented as in (A). Summary: total, 2085 Å^2; MHC + peptide, 1066 Å^2; TCR, 1019 Å^2; peptide alone, 366 Å^2.

(D) The structure of the V8A peptide represented as in (A). Summary: total, 2012 Å^2; MHC + peptide, 1010 Å^2; TCR, 1002 Å^2; peptide alone, 262 Å^2. Figure generated with RIBBONS (Carson, 1991).

Interfacial Surface Areas Vary by Only a Few Percent in Differently Signaling TCR/Tax-APL/MHC Complexes

The solvent-accessible surface area buried in an interface often gives an indication of the stability of that interface (e.g., Janin and Chothia, 1990). The difference in the solvent-accessible surface area buried in the formation of the TCR to peptide/MHC interface relative to the Tax interface is a decrease of 1% ($-$26 Å^2) and 3% (-60 Å^2) for the two weak antagonists, P6A and Y8A, and a slight increase of $<$1% ($+$12 Å^2) for the weak agonist, V7R (Figure 4A, caption). These differences are all less than the differences observed between the two agonist TCR complexes with the A6- and B7-TCRs (78 Å^2) (Figure 4A).

The solvent-accessible surface areas of the peptides Tax and P6A buried by the A6 TCR are identical (336 Å^2) (Figure 4A, caption) and are distributed over the peptide atoms identically. This implies that the two peptides are contacted essentially identically by the TCR (compare Figures 4A and 4B), but the result is a different signal, a strong agonist versus a weak antagonist.

The weak agonist peptide, V7R, has a 10% larger surface area buried by TCR than the strong agonist, Tax (Figure 4C, caption). This is due to the increased surface area of the arginine side chain that is buried in V7R relative to the valine in Tax (compare Figures 4A and 4C). This energetically favorable increase in buried surface must be balanced by the unfavorable burial of the positive charge of the guanidinium group and possibly by distortions to the TCR, to result in an almost 10-fold increase in the dissociation constant (Figure 2).

The substitution of the small alanine side chain for the large tyrosine side chain at peptide position 8 (Y8A) results in a decrease of 22% (-75 Å^2) in the peptide surface area buried by the TCR. This is almost entirely due to the loss of the contacts with the tyrosine ring and hydroxyl group (compare Figures 4A to 4D).

Changes in the overall solvent-accessible surface area buried in an interface have been estimated to contribute about 25 cal M^{-1} per Å^2 of "hydrophobic" free energy (Janin and Chothia, 1990). The largest change observed in the Tax-APL complexes (a total of 60 Å^2 of hydrophobic surface area for the Tax-Y8A structure) would only account for about 1.5 Kcal M^{-1} of the observed free energy differences of at least 2.7 Kcal M^{-1} (assuming a conservative estimate of 100 μM for the A6-TCR-HLA-A2/Tax-Y8A dissociation constant), implying that other effects discussed below are also important.

Detailed Structural Accommodations to the Peptide Substitutions in the TCR/MHC Interfaces

Antagonist Peptide P6A Shows No Structural Changes Relative to the Tax Peptide

The substitution of alanine for proline at position 6 of the peptide removes two methylene groups from the TCR to MHC/peptide interface and results in a free amide group in place of the amino group of the proline. No substantial structural alterations result in the TCR/peptide/MHC complex from this substitution (Figure 5A). The amide group of Ala-6 of the peptide is within hydrogen bonding distance of an ordered water molecule that is found in the cavity created by the removal of the proline methylene groups (Figure 5A, black sphere). The hydroxyl group of Ser-100 of CDR3α and an imidazole nitrogen from His-70 of HLA-A2 are also in the vicinity of the water and may form hydrogen bonds. The imidazole reorients by about 40°, possibly to optimize contact with the water. Leu-98 of CDR3β moves about 0.7 Å into the cavity making contact with Trp-101 of CDR3α.

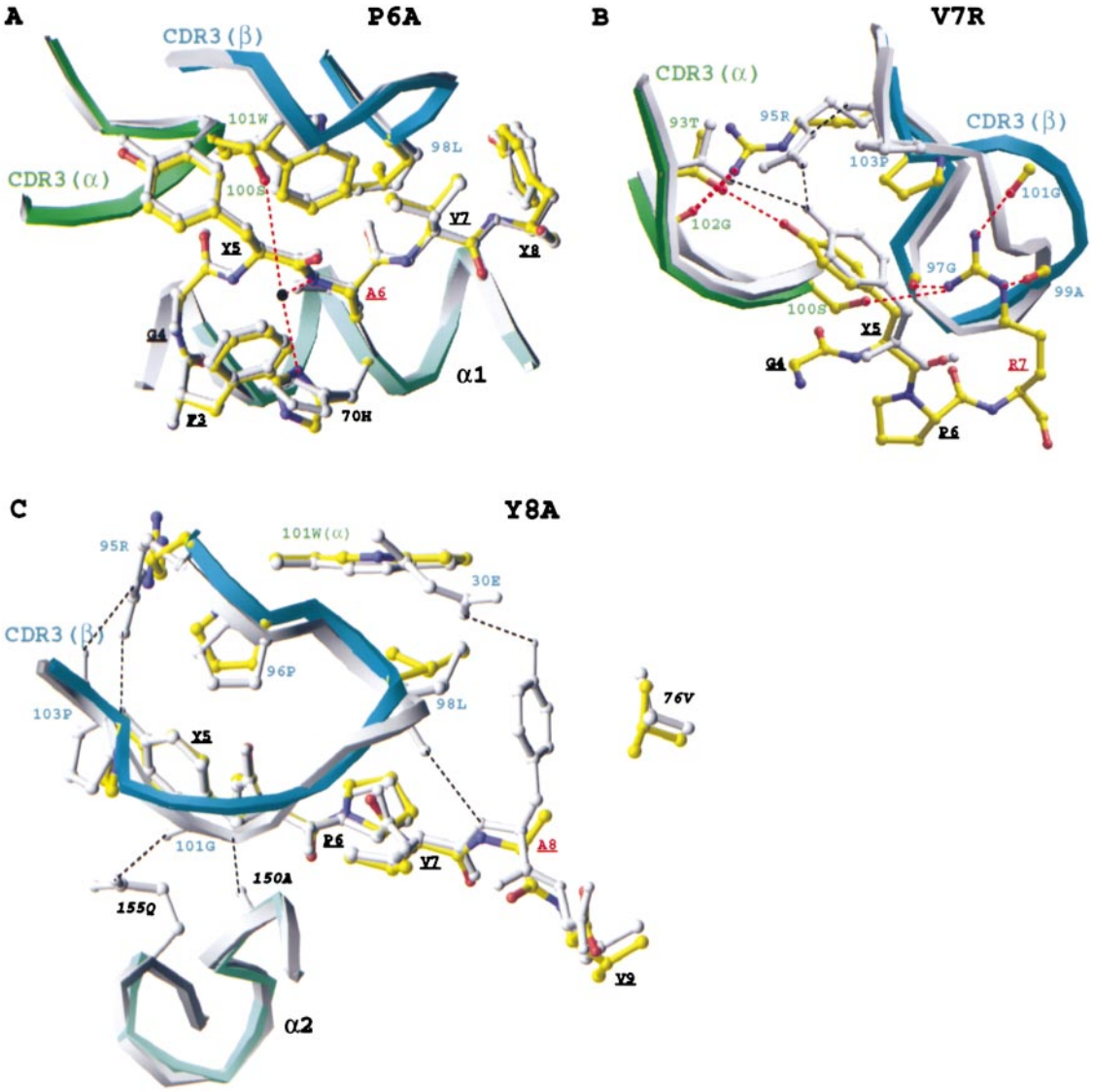

Figure 5. Structural Changes in the TCR to Tax-APL/MHC Interfaces

(A) The P6A complex (colored) superimposed on the Tax complex (gray). Potential hydrogen bonds are dashed red lines. Labels for peptide residues are underlined.

(B) The V7R complex (colored) superimposed on the Tax complex (gray).

(C) The Y8A complex (colored) superimposed on the Tax complex (gray). This figure was generated with RIBBONS (Carson, 1991).

With so little structural difference, it is difficult to rationalize the difference in half-lives between the Tax and P6A complexes, which is probably at least two orders of magnitude. The introduction of a larger cavity in the interface and the reduction in the complementarity between the TCR and MHC/peptide are probably contributing factors (see below). The observation that these complexes have such similar structures, while one is a strong activator and the other is not, is evidence that APL do not produce different signals as the result of changing the conformation of the αβTCR or the relative arrangement of the TCR and MHC molecule.

Peptide V7R Induces a Large Change in the TCR Loops but Is a Weak Agonist

The substitution of a large, positively charged arginine side chain for a valine at position 7 of the Tax peptide results in a displacement of the CDR3β loop in the A6-TCR in order to accommodate the bulky side chain in the TCR/MHC interface (Figure 5B). The guanidinium group of the arginine is surrounded by the Ser-100 hydroxyl group of CDR1α and the carbonyl oxygens of three CDR3β residues, Gly-97, Ala-99, and Gly-101, all within hydrogen-bonding distance. The three carbonyl groups apparently stabilize the buried charge of the guanidinium group by delocalizing the electrostatic charge through their solvent-accessible peptide amide groups, as previously observed for other buried charges (Quiocho et al., 1987). Gly-101 is displaced outward by 4.4 Å (Figure 5B), which allows the whole arginine side chain to be accommodated within the TCR interface.

The repositioned CDR3β loop results in the loss of two potential hydrogen bonds from Gly-101 to MHC

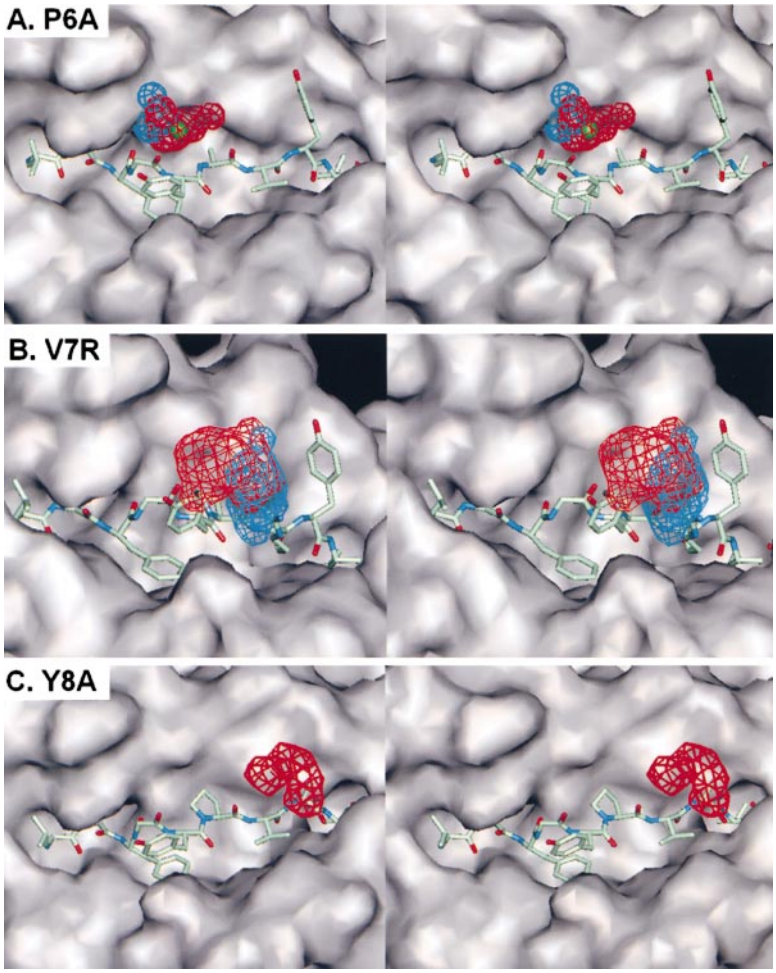

Figure 6. Cavities in the A6-TCR to Peptide/HLA-A2 Interface

(A) A cavity adjacent to peptide residue 6 is larger in the P6A complex (red mesh) than in the Tax complex (blue mesh). A bound water molecule (green) is positioned to hydrogen bond to the amide group of peptide alanine P6. The view is through the TCR onto the peptide/MHC interface. Position 1 of the Tax peptide is to the left.

(B) A cavity adjacent to peptide residue 7 is larger in the V7R complex (red mesh) than in the Tax complex (blue mesh).

(C) A cavity adjacent to peptide residue 8 is found in the Y8A complex (red mesh) but not in the Tax complex. Figure generated using the program Quanta (MSI). Gaps calculated using the program SURFNET (Laskowski, 1995).

residues 150 and 155 found in the Tax complex (Garboczi et al., 1996a) and in rearrangements in the TCR pocket that binds to Tyr-5 of Tax. The movement of the loop includes a displacement of Pro-103 by 2.3 Å (measured at Cβ), which apparently causes a displacement of Tyr-5 of the peptide. Two potential hydrogen bonds from Arg-95 are lost, one to the Tyr-5 hydroxyl group and one to the carbonyl oxygen of Pro-103. Arg-95 rearranges to form a potential hydrogen bond with the CDR3α carbonyl oxygen of G-102 (Figure 5B). Electron density corresponding to a potential water molecule is observed in a cavity introduced adjacent to Arg-95 that may make a hydrogen bond with the Nϵ atom.

The energetic costs of these large local rearrangements are difficult to assess, but the presence of flexible glycines at three positions, 97, 100, and 101, in the CDR3β loop would be expected to facilitate such an accommodation to a large peptide substitution. It is interesting to see how the burial of such a large and electrostatically charged residue was accommodated in the TCR interface with a change in dissociation constant of only 10-fold, resulting in sufficient cross-reactivity to be a weak agonist.

Peptide Y8A Induces TCR Changes Similar to V7R, the Weak Agonist, but Is Itself a Weak Antagonist

In the Tax complex, the peptide Y8 hydroxyl group was hydrogen bonded to CDR2β residue Glu-30, and the tyrosine ring made van der Waals contacts with CDR3β residue Leu-98 and MHC Val-76 (Figure 5C, gray). Removal of the tyrosine ring and replacement by an alanine side chain removes these two interactions. As a result, Glu-30 moves away from the peptide by about 0.7 Å, and Leu-98 moves 0.9 Å toward Trp-101 of CDR3α. The CDR3β loop rearrangement is similar to that in the V7R complex except the loop is displaced slightly less; for example, Gly-101 is displaced only 3.5 Å rather than 4.4 Å. The loop displacement breaks a hydrogen bond between the carbonyl oxygen of Leu-98 and the amide group of Tyr-8 of the peptide and two hydrogen bonds from the carbonyl and amide groups of Gly-101 to MHC residues 150 and 155. (The alteration of TCR to MHC contacts by single substitutions in peptide residues has been inferred earlier from T cell activation studies with murine H-2K^b/VSV-peptide ligands [Ono et al., 1998].) Arginine-95 of CDR3β is displaced, breaking hydrogen bonds to the carbonyl oxygen of residue Pro-103 across the loop and to the hydroxyl group of Tyr-5 of the peptide. The displaced Arg-95 is within hydrogen bonding distance of the CDR3α carbonyl groups of Asp-99 and Gly-102 (not shown on Figure 5C).

Although the CDR3β loop is displaced similarly in the Y8A complex as in the V7R complex, the former is an antagonist and the latter a weak agonist.

Increases in the Size of Cavities in the TCR/Peptide/MHC Interface May Account for Some of the TCR Affinity Differences

Each of the Tax-APL complexes has a new or enlarged cavity in the TCR to peptide/MHC interface as the result of a less perfect fit of the TCR to the peptide/MHC complex (Figure 6). In the Tax complex, there are two such internal cavities, one between the side chain of peptide Pro-6 and the α1-domain α helix of the MHC molecule and the other above peptide position 6 (Figures 6A and 6B, blue). In the P6A complex, the first cavity is increased in volume by 18 Å^3 (Figure 6A, red), and in V7R the second cavity is increased in volume by 40 Å^3 (Figure 6B, red). In the Y8A complex, a new cavity adjacent to the substituted residue is found with a volume of 55 Å^3 (Figure 6C, red). Enlarged and novel cavities in this interface would be expected to decrease the binding affinity of the TCR. The magnitude of that change is difficult to estimate, but studies of the stability of the native conformation of folded proteins suggest that the free energy increases by about 24 to 33 cal M^{-1} per Å^3 of cavity volume (Eriksson et al., 1992). These cavities might then be expected to reduce the stability by about 0.5 to 1.5 Kcal M^{-1}, which is at most a 10-fold effect on the equilibrium constant. (For discussion of other complicating factors, see Eriksson et al., 1992; Guo et al., 1993.) Large cavities have also been found in the structure of a weak affinity 2C-TCR/dEV8H/2K^b murine complex formed in vitro (Garcia et al., 1998).

An ordered water molecule is found in the enlarged cavity in the P6A complex within hydrogen bonding distance of the peptide amide group created by the substitution of alanine for proline at position 6 (Figure 6A, green sphere). The entropic cost of ordering bound water molecules is estimated to be from 0 to 2 Kcal M^{-1}, with the higher value applying only to very firmly bound waters (Dunitz, 1994). The high temperature factor of the water observed here (B = 50 Å^2) suggests that the entropic cost would be at the low end of this range. Thus, the observed changes in cavity volume and bound solvent probably account for only a fraction of the destabilization of the TCR dissociation constant in the different Tax-APL complexes.

Differences in the Complementarity of Fit between TCR and Tax-APL/MHC Complexes

Lawrence and Colman (1993) have described a shape complementarity function (SC) that estimates from the atomic coordinates in an interface the complementarity in curvature between two interacting protein surfaces. (The overall shape complementarity of the A6/Tax/HLA-A2 and 2C/dEV8/H-2K^b TCR/MHC complexes was reported earlier (Garcia et al., 1998; Ysern et al., 1998; but see also Garcia et al., 1999). Plots of SC on the interfaces studied here show holes in the interface in the P6A, V7R, and Y8A complexes, as well as decreases in complementarity around the peptide substitutions (B. M. B. et al., 1999, Cold Spring Harbor Symposium of Quantitative Biology, in press). In each Tax-APL complex, the rearrangements in the TCR loops resulting from the peptide substitutions at positions 6, 7, and 8 also affect the complementarity of binding at the central pocket recognizing the tyrosine-5 peptide side chain. This might be expected for a molecular interaction where the interface can adapt to achieve its best fit by small atomic displacements and has been suggested by TCR specificity studies (Ausubel et al., 1996).

Implications for TCR Signaling

The three structures of A6-TCR/HLA-A2 complexes containing singly substituted variants of the Tax peptide studied here provide direct evidence that TCR/MHC complexes that generate different signals in T cells do not have different conformations. P6A, an antagonist, is almost identical to Tax, a strong agonist. Small and similar alterations are seen in CDR3β of V7R, a weak agonist, and Y8A, an antagonist. P6A and Y8A, which differ in the overall rearrangement of the TCR domains, are both weak antagonists. Most of the structural differences are confined to TCR loops in the TCR to peptide/MHC interface where they appear to be accommodating for the changes in ligand composition (Figure 5). The differences between two different TCR, A6 and B7, bound to Tax/HLA-A2, both of which generate strong agonist signals, is much greater, both in the interface and in the overall tilt of TCR domains than that described here for the Tax-APL complexes that generate different signals.

These observations provide direct structural evidence that no particular structural arrangement of the $\alpha\beta$TCR chains relative to the MHC molecule encodes the different signaling possibilities. This conclusion is subject to the caveat that because the crystal structures contain only the α and β ectodomains of the TCR, the contributions, if any, of the δ, ϵ, γ, and ζ subunits and the transmembrane segments of all of the subunits are unknown at this time. What the current observations indicate are that no consistent structural difference is seen propagated from the peptide binding site that could carry the different messages to these other subunits that are expected to be at the base of the $\alpha\beta$TCR, surrounding the $\alpha\beta$ constant domains (Ding et al., 1998; reviewed in Garcia et al., 1999).

How does the inside of a T cell know when a TCR has engaged a peptide/MHC ligand and how does it know which signal(s) to initiate? It is clear that one peptide/MHC ligand does not physically cross-link two $\alpha\beta$TCR complexes into a 1:2 complex, analogous to the model for human growth hormone where transmission of the signal into the cell is by alteration in the relative positions of the cytoplasmic domains of the receptor molecules. Also, structural data on human and murine TCR/peptide/MHC complexes provide no evidence for conformational changes induced in TCR by binding ligand that are consistent with sending the signal that ligand engagement has occurred into the cell (Garboczi et al., 1996a; Garcia et al., 1996; Ding et al., 1998; reviewed in Garcia et al., 1999). This lack of evidence for a conformational change also argues against models where the TCR to ligand interaction triggers a conformational change that subsequently favors oligomerization or aggregation (reviewed in Sloan-Lancaster and Allen, 1996) and does not favor models where signaling differences may result from twists in TCR/MHC interface affecting coreceptor CD8 binding (Luescher et al., 1995a, 1995b; note, however, Alam et al., 1999).

The possibility that oligomerization or aggregation of TCR/MHC pairs occurs simply because TCR interaction with ligand could create a larger oligomerization surface (Brown et al., 1993) remains possible. Data indicating a correlation between the half-life of TCR/MHC complexes and the type of signal generated suggests that the persistence of the liganded state may allow assembly with coreceptors and other TCR/MHC complexes (reviewed in Davis et al., 1998). The finding that all TCR/MHC complexes crystallized to date have a similar diagonal mode of TCR interaction is consistent with a conserved assembly mechanism (Garboczi et al., 1996a; Garcia et al., 1996, 1998; Ding et al., 1998; Wang et al., 1998). Models where persistently liganded TCR complexes segregate on the membrane, without explicit oligomeric contacts (Janeway et al., 1989), for example because their mobility has been altered, are not ruled out.

The possibility that αβTCR exist on membranes as two αβ molecules connected by CD3 and ζ chains (Fernández-Miguel et al., 1999) would permit an allosteric model of signal transmission consistent with the structural data whereby the two TCR/MHC units could change position with respect to each other without changing their internal conformation (e.g., to allow two MHC molecules to engage simultaneously the two αβ TCRs in one dimeric, $(\alpha\beta TCR)_2$). When two long-lived MHC/peptide ligands were engaged to the same divalent TCR complex, the new allosteric state induced could persist long enough for further assembly to occur or for recognition of this structural transition from inside the cell. This model is analogous to models of cytokine receptor signaling involving allosteric changes in preformed divalent (dimeric) receptors (Gadella and Jovin, 1995; Naismith et al., 1995; Damjanovich et al., 1997; Livnah et al., 1999; Remy et al., 1999).

Experimental Procedures

Cytotoxicity, IFNγ, and MIP-1β Assays

T cell assays were performed as described previously (Ding et al., 1998).

TCR Downmodulation

Antigen-presenting cells (APC) were HLA-A2 transfected Hmy2.C1R cells pulsed with 1000 nM peptides for 1 hr at 37°C. APCs (1×10^5) were incubated with 1×10^5 2G4 T cells for 5 hr at 37°C. Cells were washed and stained with PE-conjugated anti-CD8 and FITC-conjugated anti-TCR (Becton-Dickinson). TCR surface expression was quantitated by the mean fluorescence intensity (MFI) of the FITC signal. Relative units were calculated as the percentage MFI relative to T cells cultured with APCs pulsed with no peptide (identified as 100).

Antagonism Assay

Mitomycin C–treated HLA-A2 transfected Hmy2.C1R cells (Ding et al., 1998) were pulsed with 1000 nM of candidate antagonist peptides for 2 hr at 37°C, washed, and 1×10^5 cells were incubated with 1×10^5 2G4 T cells for 1 hr at 37°C. Tax peptide was added at concentrations of 0.1 to 10 nM and incubated for 48 hr. Supernatants were assayed for IFNγ content as previously described (Ding et al., 1998).

Phosphorylation of TCR-Associated Signaling Components

2G4 T cells (1×10^5) were incubated for 5 min with 2×10^5 HLA-A2-Hmy2.C1R cells pulsed with 10 μM peptides. Tyrosine phosphorylation of TCR-associated chains and ZAP-70 was detected by immunoprecipitation with a polyclonal rabbit anti-ZAP-70 antisera (kindly supplied by Dr. Larry Samelson, NIH) and immunoblotting with the anti-phosphotyrosine antibody 4G10 (Upstate Biotechnology) and horseradish peroxidase-coupled goat anti-mouse IgG (Bio-Rad) as previously described (Hemmer et al., 1998). Immunoblots were developed with SuperSignal enhanced chemiluminescence (Pierce Chemical). Quantitation of the phosphotyrosine signal in bands corresponding to the ZAP-70, p32ζ, and p38ζ was performed by laser densitometry (Molecular Dynamics).

Biacore Measurements

Sequences encoding a heterodimeric coiled coil (O'Shea et al., 1993) were added to the C termini of the TCR α and β ectodomains. The cysteines encoding the interchain disulfide bond were also reintroduced, allowing formation of the interchain disulfide bond. The free cysteine at position β192 was replaced with alanine, and a free cysteine was added to the C terminus of the extended β chain for coupling the TCR to a CM5 sensor chip by thiol exchange. Measurements were performed on a Biacore 1000. All experiments were performed on at least two surfaces of different receptor densities in 10 mM HEPES, 150 mM NaCl, 3 mM EDTA, and .0005% surfactant P-20 (pH 7.4), at 25°C. For kinetic experiments, data were collected at 10 hz and the flow rate was 100 μL/min. For equilibrium experiments, the flow rate was 10 μL/min. For kinetic data analysis, identical injections over a mock cysteine surface were subtracted from the data, and the entire association and dissociation phases were included in the fit (excluding approximately 2 sec at the start of each phase). Mass transport effects were not present under any conditions studied. For equilibrium data analysis, equilibrium values were determined by averaging the response over the final 15 sec of the injection and then subtracting averaged response values from identical injections over a mock cysteine surface. Data fitting was performed using Biaevaluation 3.0 (Biacore). Extinction coefficients were determined using the Edelhoch method (Pace et al., 1995): 95839 M^{-1} cm^{-1} for HLA-A2/Tax and 84503 M^{-1} cm^{-1} for the A6-TCR construct with the coiled coil.

The residuals for the fits to the kinetic data displayed some systematic asymmetry. For the V7R interaction, much of this can be attributed to the difficulties of examining low-affinity interactions. However, this should be less of a problem for the wild-type interaction, yet similar asymmetry was observed. Fits to more complicated models did improve the residuals, but these models could be excluded due to experimental design or unrealistic parameters. We chose to include a term for linear drift in the 1:1 binding model, which resulted in improvement. However, we cannot rule out a more complicated binding scheme. We note that similar deviations from a simple 1:1 model have been observed by others examining TCR-MHC/peptide interactions by Biacore.

Crystallization, Data Collection, and Structure Determination

Crystals of the P6A, V7R, and Y8A complexes were made by mixing A6-TCR (12 mg/ml) with HLA-A2/peptide complexes, both in 10 mM MES [pH 6.5], 50 mM NaCl, and 0.5 mM EDTA, and seeding (Garboczi et al., 1996a). Seeds were made by dilution (50 mM MOPS (pH 7.0), 75 mM $MgSO_4$, and 13% PEG 8000) of crushed A6-TCR/Tax/HLA-A2 crystals. Crystals were harvested by flash cooling in liquid nitrogen (Garboczi et al., 1996a).

Diffraction data for the P6A and V7R complexes were recorded on a Mar345 detector (Mar Research) (P6A: d = 240 mm, 1° oscillation; V7R: d = 274 mm, 1° oscillation) with an Elliot GX-13 rotating anode source collimated by double mirrors (λ = 1.54 Å). Data for Y8A crystals were collected on an ADSC 2K CCD detector (0.5° oscillations, d = 125.9 mm, λ = 0.908 Å; CHESS A1 beamline). Y8A diffraction was anisotrophic, and data are incomplete near the b axis. Data were integrated and scaled with DENZO and SCALEPACK (Otwinowski and Minor, 1997) (Table 1).

The initial model included the heavy chain and β2m of HLA-A2 and the Vα, Vβ, and Cβ domains of the A6-TCR with the peptide and CDR loops (~60 residues) omitted. For the P6A complex, after rigid-body refinement, the R_{free} was .393 (R_{crys} = .359) with data from 15–3.2 Å. The reflections used to calculate R_{free} were the same set used in the refinement of the A6-TCR/Tax/HLA-A2 complex (Garboczi et al., 1996a). Electron density calculated from the rigid-body refined model showed the missing Cα domain. The Cα domain from

Table 1. Crystallographic Data

	P6A	V7R	Y8A
A. Cell Parameters (space group C2)			
a (Å)	226.95	224.86	224.67
b (Å)	48.76	48.89	48.46
c (Å)	94.55	94.46	93.74
β (deg.)	90.79	90.49	90.46
B. Data Collection			
Resolution (Å)	25.0–2.8	25.0–2.8	25.0–2.8
Mosaicity (deg.)	0.95	0.74	1.1
No. unique reflections	25752	23577	21020
Average redundancy[a]	3.1 (2.5)	2.1 (1.3)	2.2 (1.8)
Completeness (%)	98.2 (83.2)	91.6 (60.8)	87.9 (87.9)
Average I/σ	15.1 (3.7)	12.2 (1.4)	13.5 (2.3)
R_{merge}[b]	0.076 (0.26)	0.071 (0.53)	0.063 (0.215)
C. Refinement (25.0–2.8 Å all data with F > 0.0)			
No. reflections (free)[c]	23047 (2705)	21094 (2481)	18831 (2189)
R_{cryst}[d], (Rfree)	0.216 (0.273)	0.243 (0.290)	0.247 (0.287)
Rmsd bonds[e] (Å)	0.007	0.008	0.01
Rmsd angles[f] (deg.)	1.27	1.5	1.7
Ramachandran Plot[g]			
Favored (%)	83.2	79.3	79.3
Allowed (%)	16.0	18.9	19.3
Generous (%)	0.8	1.8	1.4

[a] Numbers in parentheses are for final shell 2.9–2.8 Å.
[b] $R_{merge} = \Sigma_h\Sigma_i|I_i(h) - <I(h>)|/\Sigma_h\Sigma_i I_i(h)$, where $I_i(h)$ is the i^{th} measurement and $<I(h)>$ is the weighted mean of all measurements of I(h).
[c] (free) are number of reflections in free set.
[d] R_{cryst} and $R_{free} = \Sigma_h||F(h)_{obs}|-|F(h)_{calc}||/\Sigma_h|F(h)_{obs}|$ for reflections in the working and test sets, respectively.
[e] Bond length rmsd from ideal.
[f] Bond angles rmsd from ideal.
[g] As defined in PROCHECK (Laskowski et al., 1993).

the B7-TCR/Tax/HLA-A2 structure (Ding et al., 1998) was placed into this electron density and refined as a rigid-body to an R_{free} = .379 (R_{cryst} = .349). $3F_o$-$2F_c$ and F_o-F_c electron density maps calculated from the new model were used for rebuilding. Omit maps were calculated by CNS torsion-angle dynamics refinement omitting 20–30 residues at a time (Brünger, 1992; Pannu and Read, 1996; Adams et al., 1997). Three rounds of positional refinement and manual rebuilding were carried out. During these cycles of manual rebuilding, refined models were only used to calculate R factors and new electron density maps. Electron density appeared for three loops on the Cβ domain of TCR (disordered in A6-TCR/Tax/HLA-A2). After conventional positional refinement (with an anisotrophic B factor and bulk solvent correction) using all data from 25–2.8 Å, the R_{free} was reduced to .335 (R_{cryst} = .294). The CDR loops were added and refined to R_{free} of .316 (R_{cryst} = .295). The peptide was built reducing the R_{free} to .291 (R_{cryst} = .254). Subsequent B factor refinement (group and individual) followed by conventional positional refinement reduced the R_{free} to .276 (R_{cryst} = .227). The mean B factors of P6A (α1α2, 33.6 Å^2; α3, 80.7 Å^2; β2m, 37.8 Å^2; P6A peptide, 26.8 Å^2; Vα, 40.3 Å^2; Cα, 72.7 Å^2; Vβ, 42.8 Å^2; Cβ, 65.8 Å^2) have a distribution similar to that of A6-TCR/Tax/HLA-A2 (Garboczi et al., 1996a). CNS torsion-angle dynamics simulated annealing refinement reduced the R_{free} to .273 (R_{cryst} = .216). The final model of A6-TCR/P6A/HLA-A2 contains 50 waters, 37 of which were also found in the A6-TCR/Tax/HLA-A2 structure. Weak difference electron density was observed at 11 of those 13 positions in the A6-TCR/Tax/HLA-A2 structure. Clear electron density in the P6A complex resolved ambiguities in the A6-TCR/Tax/HLA-A2 electron density maps; e.g., the sidechain of TCRβ Arg 102 and of the N terminus of the TCR α chain were remodeled in P6A, with water molecules placed in the positions originally modeled in the A6-TCR/Tax/HLA-A2 structure. For comparisons, the A6/Tax/A2 structure was remodeled at these two positions to be the same as the P6A.

The V7R and Y8A complexes were refined like the P6A complex except that the Cα domain from the P6A structure was used. The V7R complex was oriented slightly differently and located with AMoRe (Navaza and Saludjian, 1997). The final models of Y8A and V7R complexes were not refined with torsion-angle dynamics simulated annealing. For the Y8A complex, 21 water molecules were found at the same locations as in the Tax complex. Because of the quality of the data at high resolution (Table 1), no solvent was included in the V7R complex model.

Acknowledgments

We thank Irena Stefanova, National Institutes of Health (NIH), for help with the TCR-associated tyrosine phosphorylation, Ursula Utz for making the αβTCR constructs with terminal coiled coils used in the Biacore measurements, David Myszka for advice on Biacore experiments, R. Crouse, A. Haykov, S. Sluter, C. Garnett, and the staff of CHESS for technical support, and P. Ghosh, Q. Fan, L. Mosyak, R. Chopra, and other members of the Harrison/Wiley Laboratory for help. B. M. B. is supported by the Cancer Research Institute. This research was supported by the intramural NIH program, NIH grant (AI39619), and the Howard Hughes Medical Institute (HHMI). D. C. W. is an investigator of the HHMI.

Received April 26, 1999; revised May 20, 1999.

References

Adams, P.D., Pannu, N.S., Read, R.J., and Brünger, A.T. (1997). Cross-validated maximum likelihood enhances crystallographic simulated annealing refinement. Proc. Natl. Acad. Sci. USA *94*, 5018–5023.

Alam, S.M., Davies, G.M., Lin, C.M., Zal, T., Nasholds, W., Jameson, S.C., Hogquist, K.A., Gascoigne, N.R.J., and Travers, P.J. (1999). Qualitative and quantitative differences in T cell receptor binding of agonist and antagonist ligands. Immunity *10*, 227–237.

Ausubel, L.J., Kwan, C.K., Sette, A., Kuchroo, V., and Hafler, D.A. (1996). Complementary mutations in an antigenic peptide allow for crossreactivity of autoreactive T-cell clones. Proc. Natl. Acad. Sci. USA *93*, 15317–15322.

Brown, J.H., Jardetzky, T.S., Gorga, J.C., Stern, L.J., Urban, R.G., Strominger, J.L., and Wiley, D.C. (1993). Three-dimensional structure of the human class II histocompatibility antigen HLA-DR1. Nature *364*, 33–39.

Brünger, A.T. (1992). Free R value: a novel statistical quantity for assessing the accuracy of crystal structures. Nature *255*, 472–475.

Carson, M. (1991). Ribbons 2.0. J. Appl. Crystallogr. *24*, 958–961.

Damjanovich, S., Bene, L., Matko, J., Alileche, A., Goldman, C.K., Sharrow, S., and Waldmann, T.A. (1997). Preassembly of interleukin 2 (IL-2) receptor subunits on resting Kit 225 K6 T cells and their modulation by IL-2, IL-7, and IL-15: a fluorescence resonance energy transfer study. Proc. Natl. Acad. Sci. USA *94*, 13134–13139.

Davis, M.M., Boniface, J.J., Reich, Z., Lyons, D., Hampl, J., Arden, B., and Chien, Y. (1998). Ligand recognition by alpha beta T cell receptors. Annu. Rev. Immunol. *16*, 523–544.

Ding, Y.-H., Smith, K.J., Garboczi, D.N., Utz, U., Biddison, W.E., and Wiley, D.C. (1998). Two human T cell receptors bind in a similar diagonal mode to the HLA-A2/tax peptide complex using different TCR amino acids. Immunity *8*, 403–411.

Dunitz, J.D. (1994). The entropic cost of bound water in crystals and biomolecules. Science *264*, 670.

Eriksson, A.E., Baase, W.A., Zhang, X.-J., Heinz, D.W., Blaber, M., Baldwin, E.P., and Matthews, B.W. (1992). Response to a protein structure to cavity-creating mutations and its relation to the hydrophobic effect. Science *255*, 178–183.

Fernández-Miguel, G., Alarcón, B., Iglesias, A., Bluethmann, H., Alvarez-Mon, M., Sanz, E., and de la Hera, A. (1999). Multivalent structure of an abT cell receptor. Proc. Natl. Acad. Sci. USA *96*, 1547–1552.

Gadella, T.W., Jr., and Jovin, T.M. (1995). Oligomerization of epidermal growth factor receptors on A431 cells studied by time-resolved fluorescence imaging microscopy. A sterochemical model for tyrosine kinase receptor activation. J. Cell Biol. *129*, 1543–1558.

Garboczi, D.N., Hung, D.T., and Wiley, D.C. (1992). HLA-A2-peptide complexes: refolding and crystallization of molecules expressed in Escherichia coli and complexed with single antigenic peptides. Proc. Nat. Acad. Sci. USA *89*, 3429–3433.

Garboczi, D.N., Ghosh, P., Utz., U., Fan, Q.R., Biddison, W.E., and Wiley, D.C. (1996a). Structure of the complex between human T cell receptor, viral peptide, and HLA-A2. Nature *384*, 134–141.

Garboczi, D.N., Utz, U., Ghosh, P., Seth, A., Kim, J., van Tienhoven, A.E., Biddison, W.E., and Wiley, D.C. (1996b). Assembly, specific binding, and crystallization of a human TCR-$\alpha\beta$ with an antigenic tax peptide from human T lymphotropic virus type 1 and the class I MHC molecule HLA-A2. J. Immunol. *157*, 5403–5410.

Garcia, K.C., Degano, M., Stanfield, R.L., Brunmark, A., Jackson, M.R., Peterson, P.A., Teyton, L., and Wilson, I.A. (1996). An ab T cell receptor at 2.5 Å and its orientation in the TCR-MHC complex. Science *274*, 209–219.

Garcia, K.C., Degano, M., Pease, L.R., Huang, M., Peterson, P.A., Teyton, L., and Wilson, I.A. (1998). Structural basis of plasticity in T cell receptor recognition of a self peptide-MHC antigen. Science *279*, 1166–1172.

Garcia, K.C., Teyton, L., and Wilson, I.A. (1999). Structural basis of T cell recognition. Annu. Rev. Immunol. *17*, 369–397.

Guo, H.-C., Madden, D.R., Silver, M.L., Jardetzky, T.S., Gorga, J.C., Strominger, J.L., and Wiley, D.C. (1993). Comparison of the P2 specificity pocket in three human histocompatibility antigens: HLA-A*6801, HLA-A*0201 and HLA-B*2705. Proc. Natl. Acad. Sci. USA *90*, 8053–8057.

Hausmann, S., Biddison, W.E., Smith, K.J., Ding, Y.H., Garboczi, D.N., Utz, U., Wiley, D.C., and Wucherpfennig, K.W. (1999). Peptide recognition of two HLA-A2/Tax(11–19) specific T-cell clones in relationship to their MHC/peptide/TCR crystal structures. J. Immunol. *162*, 5389–5397.

Hemmer, B., Stefanova, I., Vergelli, M., Germain, R.N., and Martin, R. (1998). Relationships among TCR ligand potency, thresholds for effector function elicitation, and the quality of early signaling events in human T cells. J. Immunol. *160*, 5807–5814.

Janeway, C.A., Jr., Dianzani, U., Portoles, P., Rath, S., Reich, E.-P., Rojo, J., Vagi, J., and Murphy, D.P. (1989). Cross-linking and conformational change in T-cell receptors: role in activation and in repertoire selection. Cold Spring Harbor Symp. Quant. Biol. *54*, 657–666.

Janin, J., and Chothia, C. (1990). The structure of protein-protein recognition sites. J. Biol. Chem. *265*, 16027–16030.

Laskowski, R.A. (1995). SURFNET: a program for visualizing molecular surfaces, cavities and intermolecular interactions. J. Mol. Graph. *13*, 323–330.

Lawrence, M.C., and Colman, P.M. (1993). Shape complementarity at protein/protein interfaces. J. Mol. Biol. *234*, 946–950.

Livnah, O., Stura, E.A., Middleton, S.A., Johnson, D.L., Jolliffe, L.K. and Wilson, I.A. (1999). Crystallographic evidence for preformed dimers of erythropoietin receptor before ligand activation. Science *283*, 987–990.

Ljunggren, H.-G., Stam, N.J., Ohlen, C., Neefjes, J.J., Hoglund, P., Heemels, M.-T., Bastin, J., Schumacher, T.N.M., Townsend, A., Karre, K., and Ploegh, H.L. (1990). Empty MHC class I molecules come out in the cold. Nature *346*, 476–480.

Luescher, I.F., Anjuere, F., Peitsch, M.C., Jongeneel, C.V., Cerottini, J.C., and Romero, P. (1995a). Structural analysis of TCR-ligand interactions studied on H-2Kd-restricted cloned CTL specific for a photoreactive peptide derivative. Immunity *3*, 51–63.

Luescher, I.F., Vivier, E., Layer, A., Mahiou, J., Godeau, F., Malissen, B., and Romero, P. (1995b). CD8 modulation of T-cell antigen receptor-ligand interactions on living cytotoxic T lymphocytes. Nature *373*, 353–356.

Madden, D.R., Garboczi, D.N., and Wiley, D.C. (1993). The antigenic identity of peptide-MHC complexes: a comparison of the conformations of five viral peptides presented by HLA-A2 [published erratum appears in Cell 1994 Jan 28;76(2):following 410]. Cell *75*, 693–708.

Madrenas, J., Wange, R.L., Isakov, J.L., Samelson, L.E., and Germain, R.N. (1995). Zeta phosphorylation without ZAP-70 activation induced by TCR antagonists or partial agonists. Science *267*, 515–518.

Naismith, J.H., Devine, T.Q., Brandhuber, B.J., and Sprang, S.R. (1995). Crystallographic evidence for dimerization of unliganded tumor necrosis factor receptor. J. Biol. Chem. *270*, 13303–13307.

Navaza, J., and Saludjian, P. (1997). AMoRe: an automated molecular replacement program package. Methods Enzymol. *276*, 581–594.

Ono, T., DeLorenzi, T.P., Wang, F., Kalergis, A.M., and Nathenson, S.G. (1998). Alterations in TCR-MHC contacts subsequent to cross-recognition of class I MHC and singly substituted peptide variants. J. Immunol. *161*, 5454–5463.

O'Shea, E.K., Lumb, K.J., and Kim, P.S. (1993). Peptide velcro: design of a heterodimeric coiled coil. Curr. Biol. *3*, 658.

Otwinowski, Z., and Minor, W. (1997). Processing of X-ray diffraction data collected in oscillation mode. Methods Enzymol. *276*, 307–326.

Pace, C.N., Vajdos, F., Fee, L., Grimsley, G., and Gray, T. (1995). How to measure and predict the molar absorption coefficient of a protein. Protein Sci. *4*, 2411–2423.

Pannu, N.S., and Read, R.J. (1996). Improved structure refinement through maximum likelihood. Acta Crystallogr. *A52*, 659–668.

Quiocho, F., Sack, J.S., and Vyas, N.K. (1987). Stabilization of charges on isolated ionic groups sequestered in proteins by polarized peptide units. Nature *329*, 561–564.

Remy, I., Wilson, I.A., and Michnick, S.W. (1999). Erythropoietin receptor activation by a ligand-induced conformation change. Science *383*, 990–993.

Roman, G.C., and Osame, M. (1988). Identity of HTLV-1-associated tropical spastic paraparesis and HTLV-1-associated myelopathy. Lancet *1*, 651.

Sloan-Lancaster, J., and Allen, P.M. (1996). Altered peptide ligand-induced partial T cell activation: molecular mechanisms and role in T cell biology. Annu. Rev. Immunol. *14*, 1–27.

Sloan-Lancaster, J., Shaw, A.S., Rothbard, J.B., and Allen, P.M. (1994). Partial T cell signaling: altered phospho-zeta and lack of ZAP-70 recruitment in APL-induced T cell anergy. Cell *79*, 913–922.

Utz, U., Banks, D., Jacobson, S. and Biddison, W.E. (1996). Analysis of the T-cell receptor repertoire of human T-cell leukemia virus type 1 (HTLV-1) Tax-specific CD8+ cytotoxic T lymphocytes from patients with HTLV-1-associated disease: evidence for oligoclonal expansion. J. Virol. *70*, 843–851.

Valitutti, S., Muller, S., Cella, M., Padovan, E., and Lanzavecchia, A. (1995). Serial triggering of many T-cell receptors by a few peptide-MHC complexes. Nature *375*, 148–151.

Wang, J.-h., Lim, K., Smolyar, A., Teng, M.-k., Liu, J.-h., Tse, A.G.D., Liu, J., Hussey, R.E., Chishti, Y., Thomson, C.T., et al. (1998). Atomic structure of an ab T cell receptor (TCR) heterodimer in complex with an anti-TCR Fab fragment derived from a mitogenic antibody. EMBO J. *17*, 10–26.

Ysern, X., Li, H., and Mariuzza, R.A. (1998). Imperfect interfaces. Nat. Struct. Biol. *5*, 412–414.